Buoyancy limits and ascending velocity of lean syngas flames

Ballossier Y.[1], Desclaux A.[1], Bouton M.[1], Bentaib A.[2], Comandini A.[1], Chaumeix N.[1]
[1] ICARE, UPR 3021 CNRS, Orléans, France
[2] ASNR, Fontenay-aux-Roses, France

1 Introduction

Syngas composed of di-hydrogen, H_2, and carbon monoxide, CO, is present in many industrial systems. Sometimes intentionally by gasification of coal or biomass pyrolysis, or unintentionally inside a nuclear reactor. Indeed, in the event of a reactor runaway, the exothermic oxidation of metallic components produces H_2 (early phase) and the interaction of the corium with the concrete forms CO (late phase). This could lead to the formation of a hot H_2+CO mixture, while passive systems reduce the concentration of H_2 and O_2, causing oxygen starvation. Depending on the accident scenarios, a stratification of the combustible concentration occurs with a lean mixture at the bottom near the core and a richer mixture at the top of the confinement chamber. We focus here on this particular scenario where a lean mixture close to the flammability limits is ignited and forms a rising flame kernel due to buoyancy forces. If this hot core rises toward a higher concentration of combustible mixture, this could promote a fast combustion and even lead to transition from deflagration to detonation. Understanding the behaviour of buoyant flames is necessary to improve numerical models and prevent such a scenarios.

Previous work has investigated buoyant flames with other mixtures. For example, numerical simulations of rich H_2 air and CH_4 flames [1] examined the dependence of the rising velocity on the Richardson number. The authors found that curvature and strain rate are independent of each other, in contrast to spherical flames where they are linearly dependent. Experimental buoyant hydrogen-air flames [2] were observed between 60 kPa and 500 kPa. By decreasing the equivalent ratio, the authors observed a decrease in cellular instability in favour of buoyancy. An increase in pressure induces a higher buoyant flame lift and, as the equivalent ratio decreases, the flame start to rise at a lower radius. Choi et al. [3] identified different regimes of propagation of R134a/CH_4/O_2/N_2 flames within a spherical bomb. No instabilities were observed at the flame surface. The three regimes are: (i) spherical flames; (ii) buoyancy induced regime; and (iii) transition regime in between. They proposed a model for the rate of ascent with a link to the Froude number (inertial/gravitational forces) and a criterion based on the Damköhler number, which is the ratio of the time scales between the residence time (link to the rate of ascent) and the chemical time. Experimental flames under microgravity conditions [4] of highly N_2 diluted ethanol is used on a zero-gravity (0G) flight (A310) to prevent buoyancy from attaching. On Earth the flame is strongly distorted into a mushroom shape by buoyancy, but in 0G it remains spherical throughout its propagation.

Here we present an experimental study of H_2-CO buoyant flames in a spherical bomb at different initial pressures and higher dilutions of N_2 than in air, to mimic conditions relevant to an accident scenario.

Correspondence to: yves.ballossier@cnrs-orleans.fr

2 Experimental setup

A detailed description of the experimental set up and methodology used are available in [5, 6]. A brief summary is provided here for completeness.

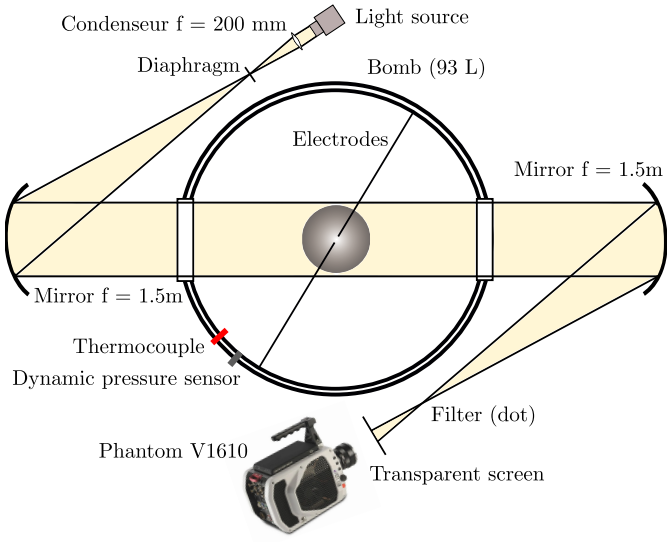

Figure 1: Experimental set-up

The apparatus (Fig. 1) is a stainless-steel spherical bomb (BS III) with double layer walls between which a heat transfer fluid can circulate to regulate the temperature. The spherical combustion chamber has an inner diameter of 563 mm. The enclosure is equipped with two pairs of quartz windows with diameters of 200 mm, situated diametrically opposed to one another. The air and fuel composition are 20.9% O_2+79.1%N_2 and 50.03% H_2 + 49.97% CO. The mixture is prepared by the partial pressure method using a MKS 690A ($\pm$0.1 Torr), leading to a relative error on fuel and oxygen mole fractions of 0.023% and 0.017%. Two Type K thermocouples measure the initial temperature inside and on the wall of the combustion chamber with a precision of $\pm$2 K. A Kistler type 6001 high-frequency pressure transducer measures the dynamic pressure during combustion. The arc energy formed between the two tungsten electrodes (2 mm diameter) for the ignition is around 10 mJ. The flame expansion is visualized via a schlieren set-up and recorded with a high-speed camera Phantom V1610. The flame radius (R_f) is deduced from the total flame area (A_f) as $R_f = \sqrt{(A_f/\pi)}$. Laminar burning speed relative to burned gas ($S_{l,b}$) is thus derived from $S_{l,b} = \dfrac{dR_f}{dt}$. No pressure rise where recorded before the flame reach the edges of the windows. The total data set consists of 93 tests.

3 Results and discussion

3.1 Morphology of buoyant flames

Freely propagating flames typically develop as spherical flames as shown on Fig. 2 for the cases with larger ($x_{fuel} \geq 13\%$) combustible concentrations in regular air ($xO_2/xN_2 = 0.276$), at ambient and elevated temperature. The flames depicted on Fig. 2 were plotted at the maximum radius before the flame reaches the edge of the window. As the combustible concentration decreases, the buoyancy effect begins to appear as the flame propagates unequally to the top and bottom of the bomb. This leads to an

upward movement of the flame from the electrodes to the top of the bomb. As the oxygen concentration is reduced, the buoyancy effects affect the flame for higher fuel concentrations and all flames become buoyant at $x_{fuel} \geq 15\%$ for a ratio of $xO_2/xN_2 = 0.06$. On the contrary, increasing the temperature delays the upward movement of the flame.

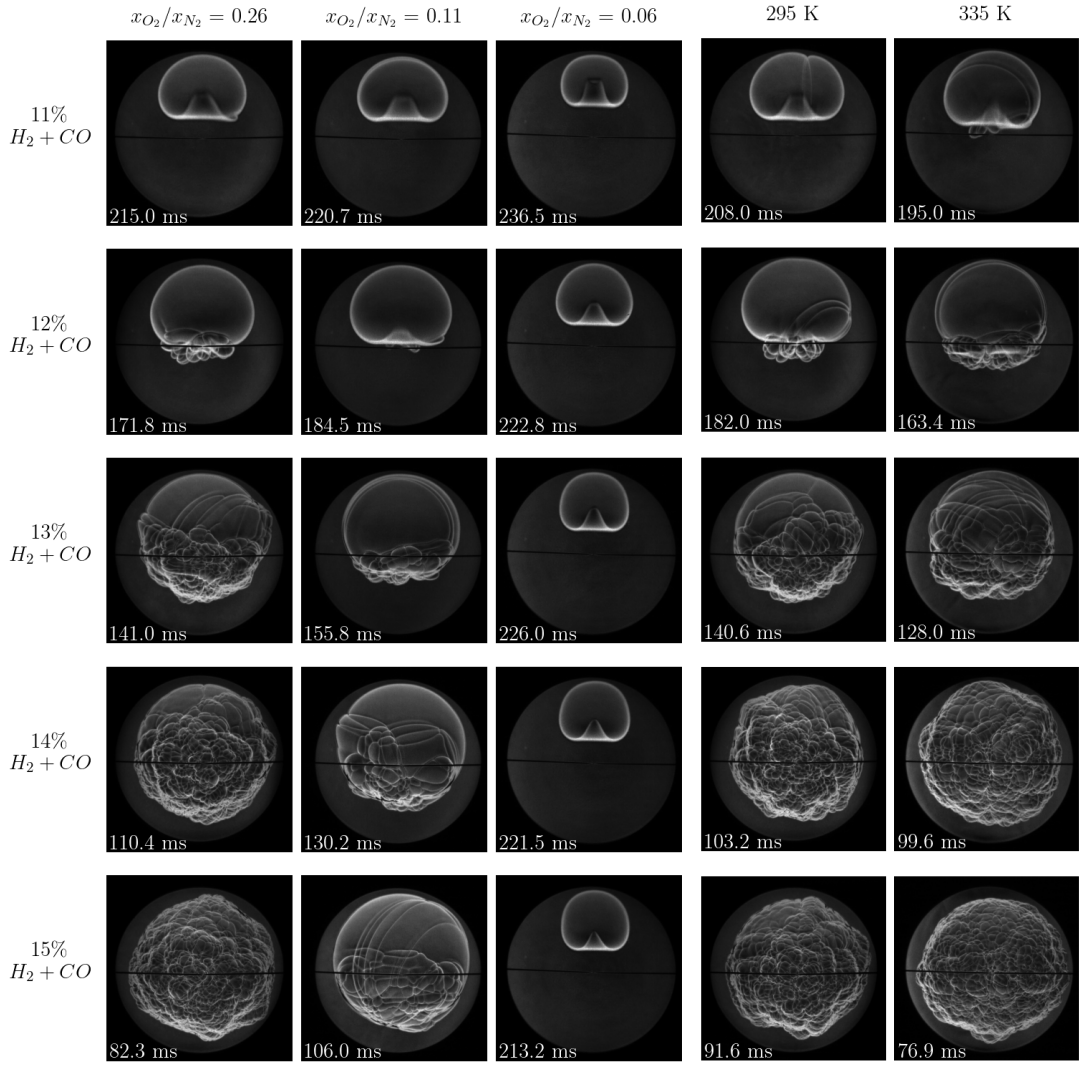

Figure 2: Morphology of H_2+CO flame from raw schlieren images when the flame reaches the edge of the observation window. Columns : 1-3 influence of oxygen starvation; 4-5 influence of initial temperature in air. Columns 1 and 4 are the same conditions but different tests. Time refers to the time elapsed since ignition.

Numerical simulations [1, 7] showed that the buoyant flame displacement pushes the fresh mixture at the top to the bottom, inducing a vortex motion around the flame. This fresh mixture vortex, which is characteristic of Rayleigh-Taylor instabilities, forces the inversion of the lower part of the flame into a concave shape. In cases where the buoyancy affects the flame only mildly (e.g. at $12\% x_{fuel}$ in air at ambient conditions), only the lower part of the flame is corrugated, while the upper part remains smooth. For fully buoyant flames, the surface remains smooth except for the lower part which may be subject to Rayleigh-Taylor instabilities, resulting in a jellyfish flame structure as seen in Fig. 2. The exact reason why the buoyant flame does not show characteristic cellular instabilities (especially for these low Lewis

mixtures) is not known but is also reported in [3].

3.2 Threshold for buoyancy driven flames

The first consideration for safety is under what conditions can buoyant flames occur? Different criteria based on dimensionless number analysis have been used in the literature such as: Rayleigh and Peclet number [8], float rate and critical flame radius [2], or Froude and Damköhler number [3]. Most studies of buoyant flames [1,4,9] use the Richardson number defined as $Ri = \frac{\rho_f - \rho_b}{\rho_f} \frac{gL}{S_{l,b}^{0\,2}}$, which is the ratio of the Archimedes' buoyancy to the characteristic velocity of the flame. The densities of the fresh and burnt mixture are given as ρ_f and ρ_b respectively, g is the gravitational acceleration, L is a characteristic length scale and $S_{l,b}^0$ is the calculated (from Cantera [10] with USC mechanism [11]) unstretched laminar flame velocity relative to the burnt gas. While all cited references observe an increase in Ri as flames become more buoyant, there is no critical value that separates clearly spherical flames from buoyant flames. Furthermore, the characteristic length scale L and velocity change from one reference to another. For example, $L = R_f$ in [1,4,9] and $L = z_c$ the distance between the centroid of the flame and the ignition point [3, 12]. We calculated the Ri number using different characteristic velocity and length scales. In all cases we observed a trend like the one shown in Fig. 3 left (with $L = R_f$). Berger et al. [1] also compared the effect of dR_f/dt instead of $S_{l,b}^0$ and found no significant difference either (but they did not compare the characteristic length).

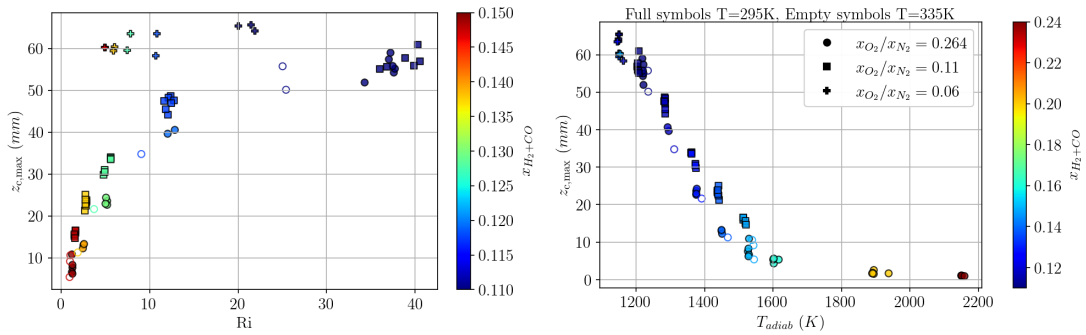

Figure 3: Left : Richardson number as a function of the maximum centroid $z_{c,max}$ vertical position. Right : adiabatic flame temperature as a function of $z_{c,max}$ (note that the fuel range is extended).

The Richardson number increases with the maximum centroid position, but even for Ri ≥ 5 we can still have a flame lifted by 35 mm, questioning the relevance of Ri as a criterion for buoyancy flames. A relevant parameter would be the ratio of $S_{l,b}^0$ to the rising velocity of the centroid V_z. Indeed, we have also observed that if the flame speed is too small, the buoyancy overtakes the chemical time scale, as shown in [3]. But it is not a simple task to determine V_z *a priori*. Instead we used the adiabatic flame temperature, T_{adiab}. After a cross-correlation test, we found that the Zeldovich number gave the better correlation factor with z_c (if we remove adimensioned numbers that cannot be calculated *a priori*). But the activation energy does not follow the evolution of z_c, whereas T_{adiab} alone gives a good criterion (and can be calculated from a simple equilibrium calculation). The result is shown in Fig 3 on the right, with an extended range of fuel concentrations to highlight the threshold. With $T_{adiab} \leq 1600K$, buoyancy begins to affect the flame, which rises accordingly. This threshold works for the H_2-CO mixture but is dimensioned and unlikely to be universal. A more rigorous approach would be to compare this temperature with the crossover temperature where the branching rate is equal to the recombination step [13].

3.3 Ascending velocity

The determination of the ascending velocity is necessary to model the displacement of the flame kernel from a region of low concentration to one of higher concentration, resulting in greater flame acceleration. Cases where the centroid did not reach 10 mm for the electrodes were filtered out to focus on buoyant flames. The centroid position of the flame is determined from the flame contour extracted from the images. The vertical position of the centroid, z_c, is fitted to a spline function and derived to obtain its velocity V_z as shown in Fig. 4 left.

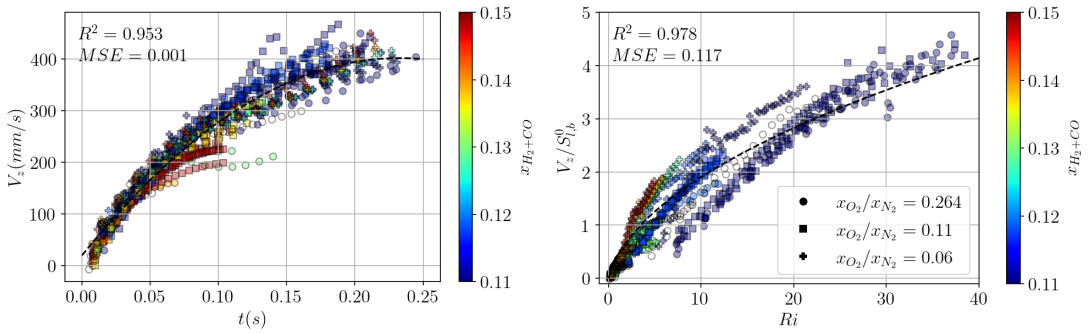

Figure 4: Centroid position. Right : as a function of time with a polynomial fit; Left : as a function of the Richardson number with the fit from Eq. 1. Dotted black lines represent the best fit.

Berger et al. [1] compare their numerical result with the prediction from a model of an air bubble rising in a water column to obtain Eq. 1. This equation is obtained from the balance of weight, buoyancy and drag forces expressed in terms of the Kelvin impulse. The experimental results are fitted to Eq. 1 as a function of c_d, which represents the drag coefficient of the flame, to find the best parameter as shown in Fig. 4 on the right. A value of $c_d = 5.18$ was obtained with our data, which is closer than the theoretical model of 6 [14].

$$\frac{V_z}{S^0_{l,b}} = \frac{2}{3}\left[\sqrt{\frac{6}{c_d}Ri + (\frac{6}{c_d})^2} - \frac{3}{c_d}\right] \tag{1}$$

While this equation is satisfactory for the physical interpretation of the phenomena, we still need to be able to calculate the Ri number, and thus the flame radius. Therefore, a second order polynomial has been fitted to Fig. 4 left and gives $V_z = 0.02 + 3.27t - 7.02t^2$ with a $R^2 = 0.953$ and a mean square error (MSE) of 0.001. This relationship gives an order of magnitude of V_z that is valid up to saturation of the rising velocity. Indeed, on Fig. 4 left we see that V_z reaches $\sim$ 200 mm/s for 15%H_2+CO in dilute air, while V_z continues to rise for lower concentrations (up to 400 mm/s in our visualisation window). On Fig. 2 we see that the flame is corrugated, which increases the flame velocity and overtakes the buoyancy effect, reducing V_z.

4 Conclusion

Spherical bomb experiments with H_2-CO mixture at different temperatures and nitrogen dilutions have been performed to investigate the buoyancy effect of the flame inside a nuclear reactor. A threshold based on the adiabatic flame temperature allows to discriminate spherical and buoyant flames more efficiently than the Richardson number, which cannot be calculated *a priori*. A comparison with the existing model

gave some insight into the mechanism rising the flame and a way to compute its velocity. Some work needs to be done to establish a universal threshold based on the crossover temperature. In addition, a specific model for a freely rising hot bubble needs to be developed to differentiate between the effect of buoyancy and the basic flame properties in order to measure the relevant flame speed for really lean mixtures. Such model would determine if the observed refractive index variation via schlieren is always due to combustion or just a hot burned gas bubble produce by the ignition.

Acknowledgements

The work was part of the AMHYCO project, which received funding from the Euratom research and training program 2019-2020 (Grant n°945057). The content of this paper reflects only the authors' view. The European Commission is not responsible for any use that may be made of the information it contains.

References

[1] L. Berger, R. Hesse, K. Kleinheinz, M. J. Hegetschweiler, A. Attili, J. Beeckmann, G. T. Linteris, H. Pitsch, A dns study of the impact of gravity on spherically expanding laminar premixed flames, Combustion and Flame 216 (2020) 412–425. doi:https://doi.org/10.1016/j.combustflame.2020.01.036.

[2] Z.-Y. Sun, G.-X. Li, H.-M. Li, Y. Zhai, Z.-H. Zhou, Buoyant unstable behavior of initially spherical lean hydrogen-air premixed flames, Energies 7 (8) (2014) 4938–4956. doi:https://doi.org/10.3390/en7084938.

[3] B. C. Choi, J. S. Park, A. F. Ghoniem, Characteristics of outwardly propagating spherical flames of r134a(c2h2f4)/ch4/o2/n2 mixtures in a constant volume combustion chamber, Energy 95 (2016) 517–527. doi:https://doi.org/10.1016/j.energy.2015.11.043.

[4] C. Bariki, F. Halter, R. Hesse, C. Chauveau, H. Pitsch, J. Beeckmann, Experimental measurements of laminar flame speeds for highly n2-diluted ethanol flames under microgravity conditions, Proceedings of the Combustion Institute 39 (3) (2023) 3929–3938. doi:https://doi.org/10.1016/j.proci.2022.08.076.

[5] J. Goulier, N. Chaumeix, F. Halter, N. Meynet, A. Bentaïb, Experimental study of laminar and turbulent flame speed of a spherical flame in a fan-stirred closed vessel for hydrogen safety application, Nuclear Engineering and Design 312 (2017) 214–227, 16th International Topical Meeting on Nuclear Reactor Thermal Hydraulics. doi:https://doi.org/10.1016/j.nucengdes.2016.07.007.

[6] A. Desclaux, M. Idir, A. Comandini, A. Bleyer, A. Bentaib, N. Chaumeix, Experimental study on turbulent flame speed of h2-co/air mixtures relevant to late phase accident scenario, 28^{th} ICDERS (2022).
URL http://www.icders.org/ICDERS2022/abstracts/ICDERS2022-173.pdf

[7] I. Yakovenko, M. Ivanov, A. Kiverin, K. Melnikova, Large-scale flame structures in ultra-lean hydrogen-air mixtures, International Journal of Hydrogen Energy 43 (3) (2018) 1894–1901. doi:https://doi.org/10.1016/j.ijhydene.2017.11.138.

[8] L. F. Alvarez, J. Shaffer, C. E. Dumitrescu, O. Askari, Laminar burning velocity of ammonia/air mixtures at high pressures, Fuel 363 (2024) 130986. doi:https://doi.org/10.1016/j.fuel.2024.130986.

[9] Z. Chang, F. Cheng, C. Wang, Z. Luo, Effects of buoyancy on the spherical flame and explosion pressure of a ch4 mixture under dilution conditions, Fuel 375 (2024) 132604. doi:https://doi.org/10.1016/j.fuel.2024.132604.

[10] D. G. Goodwin, H. K. Moffat, I. Schoegl, R. L. Speth, B. W. Weber, Cantera: An object-oriented software toolkit for chemical kinetics, thermodynamics, and transport processes, https://www.cantera.org, version 3.0.0 (2023). doi:10.5281/zenodo.8137090.

[11] S. G. Davis, A. V. Joshi, H. Wang, F. Egolfopoulos, An optimized kinetic model of h2/co combustion, Proceedings of the Combustion Institute 30 (1) (2005) 1283–1292. doi:https://doi.org/10.1016/j.proci.2004.08.252.

[12] C. Law, G. Faeth, Opportunities and challenges of combustion in microgravity, Progress in Energy and Combustion Science 20 (1) (1994) 65–113. doi:https://doi.org/10.1016/0360-1285(94)90006-X.
URL https://www.sciencedirect.com/science/article/pii/036012859490006X

[13] P. Boivin, A. L. Sánchez, F. A. Williams, Explicit analytic prediction for hydrogen–oxygen ignition times at temperatures below crossover, Combustion and Flame 159 (2) (2012) 748–752. doi:https://doi.org/10.1016/j.combustflame.2011.08.019.
URL https://www.sciencedirect.com/science/article/pii/S0010218011002689

[14] M. Zingale, L. J. Dursi, Propagation of the first flames in type ia supernovae, The Astrophysical Journal 656 (1) (2007) 333. doi:https://doi.org/10.1086/510306.